Supporting Information

Mechanically strong multifunctional three-dimensional crosslinked aramid nanofiber/holey graphene and aramid nanofiber/holey graphene/polyaniline hydrogels and derived films

Yubo Zou, Zeyu Chen, Zhiyuan Peng, Chuying Yu, Wenbin Zhong*

College of Materials Science and Engineering, Hunan University, Changsha 410082, China

*Corresponding Author: wbzhong@hnu.edu.cn (W. Zhong)

Figure S1. Illustration of the preparation of ANF dispersion from Kevlar nanofibers.

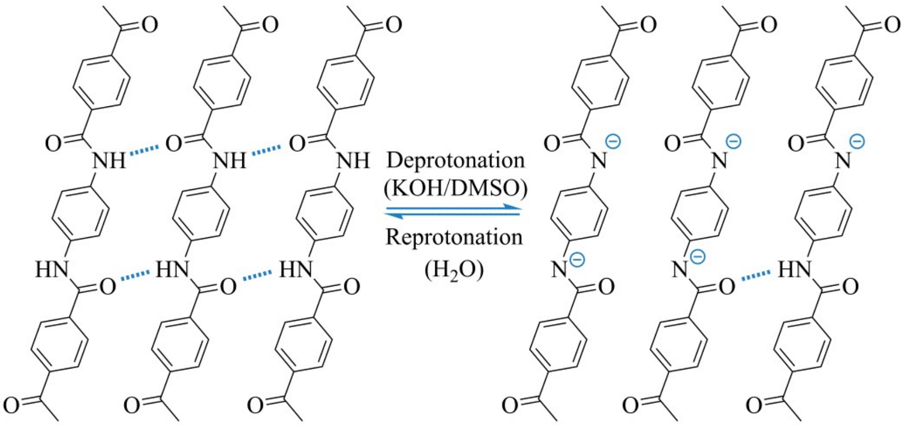

Figure S2. The deprotonation and reprotonation process of PPTA.

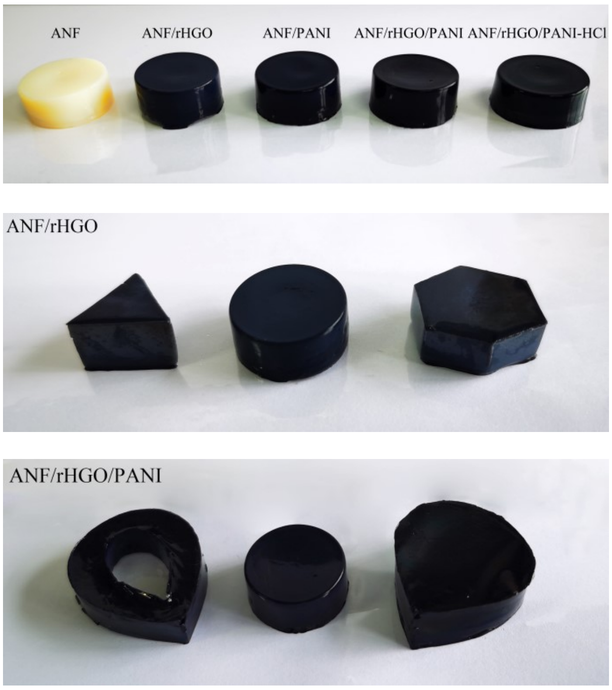

Figure S3. Illustrations of as-prepared hydrogel samples (upper), ANF/rHGO hydrogels (middle) and ANF/rHGO/PANI hydrogels (bottom) in different shapes casting from different models.

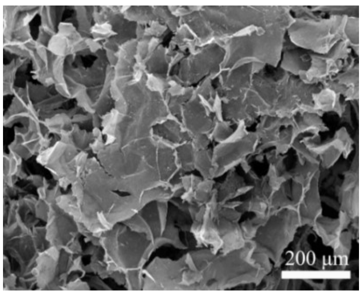

Figure S4. The SEM image of ANF/rHGO/PANI aerogel.

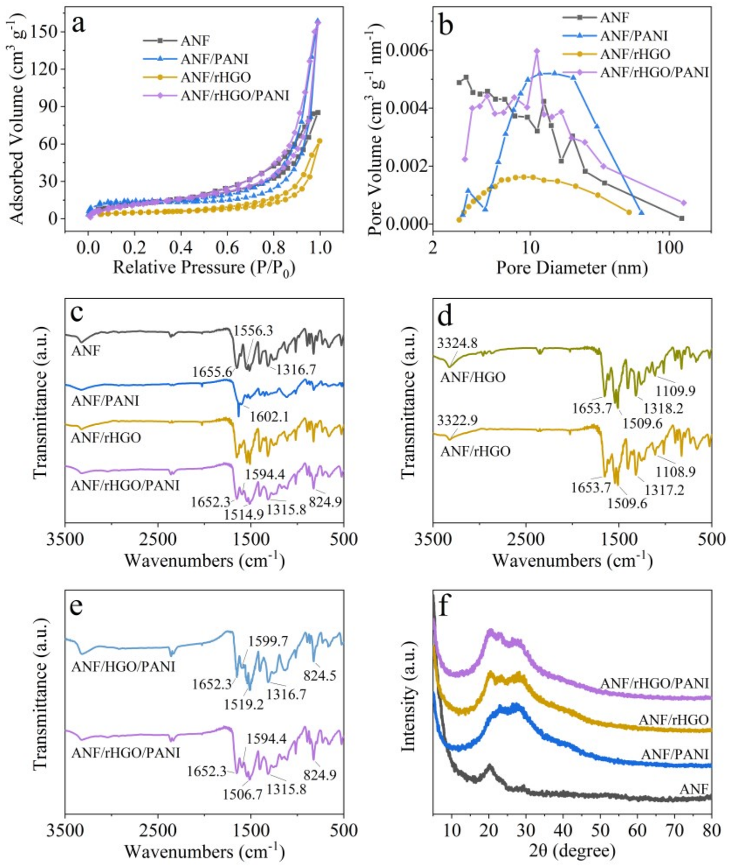

Figure S5. a) Adsorption-desorption isotherm curves, b) the pore size distribution by the BJH method, c-e) FT-IR spectra, f) XRD patterns.

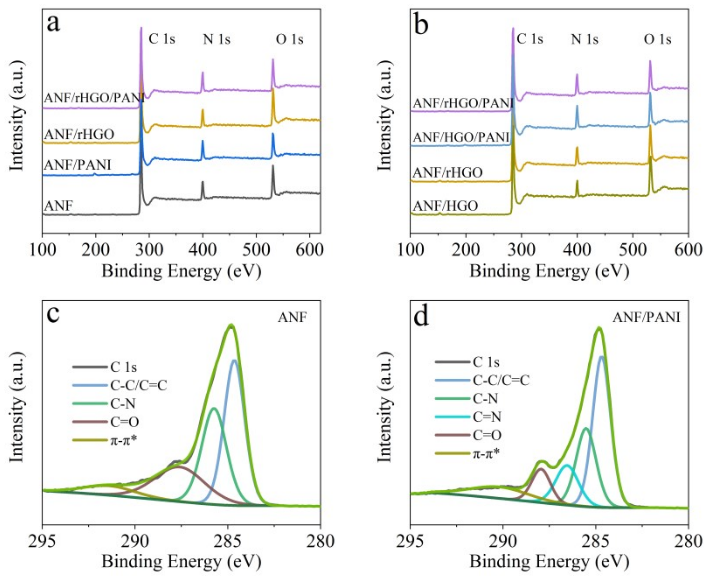

Figure S6. a-b) XPS spectra of as-prepared samples. c-d) C 1s spectra of c) ANF, d) ANF/PANI.

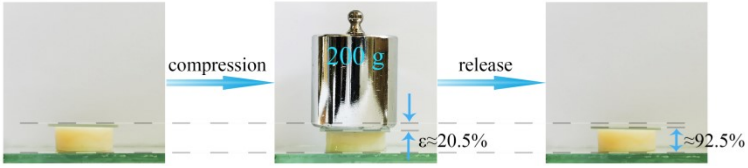

Figure S7. The compressive process for ANF hydrogel.

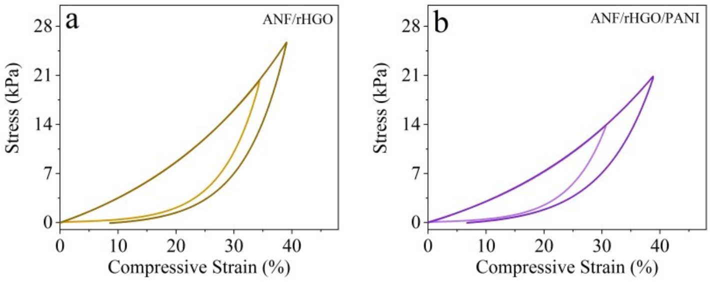

Figure S8. Compressive stress-strain curves with different strains for ANF/rHGO and ANF/rHGO/PANI hydrogels.

Figure S9. Illustration of ANF aerogel on setaria.

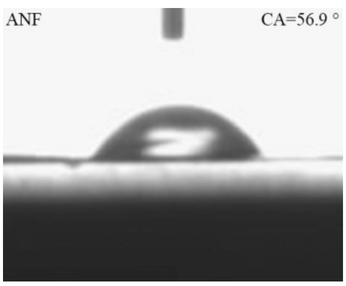

Figure S10. Illustration of static water contact angle on ANF film.

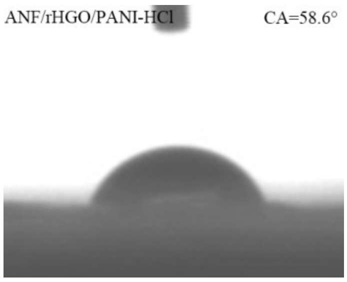

Figure S11. Illustration of static water contact angle on ANF/rHGO/PANI film after treating with 1 M HCl.

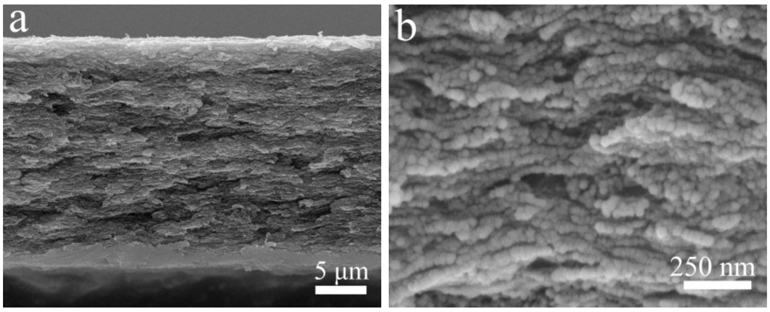

Figure S12. The SEM images of the rHGO/PANI film.

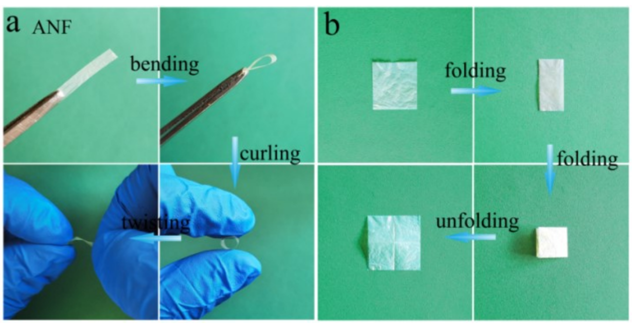

Figure S13. Illustrations of various mechanical states (initial, bending, folding, curling and twisting) of flexible ANF films.

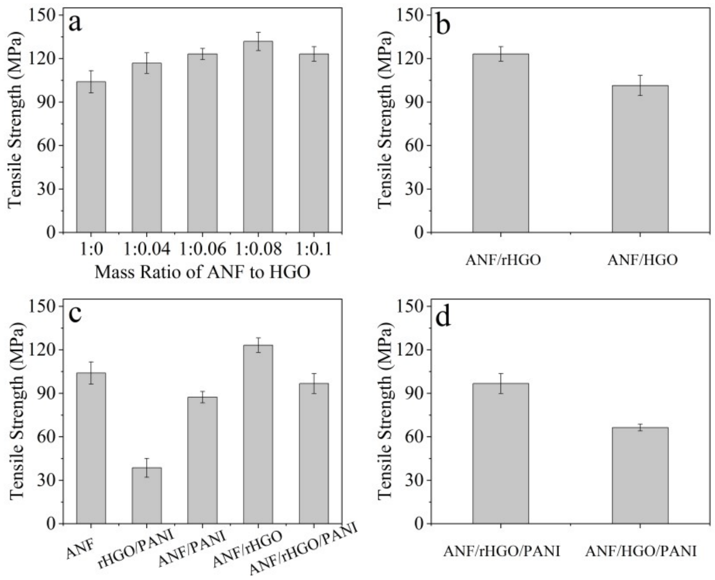

Figure S14. Averaged breaking tensile strength of (a) ANF/rHGO films with different mass ratios of ANF to HGO, (b) comparison of ANF/rHGO and ANF/HGO films, (c) as-prepared flexible films and (d) comparison of ANF/rHGO/PANI and ANF/HGO/PANI film samples.

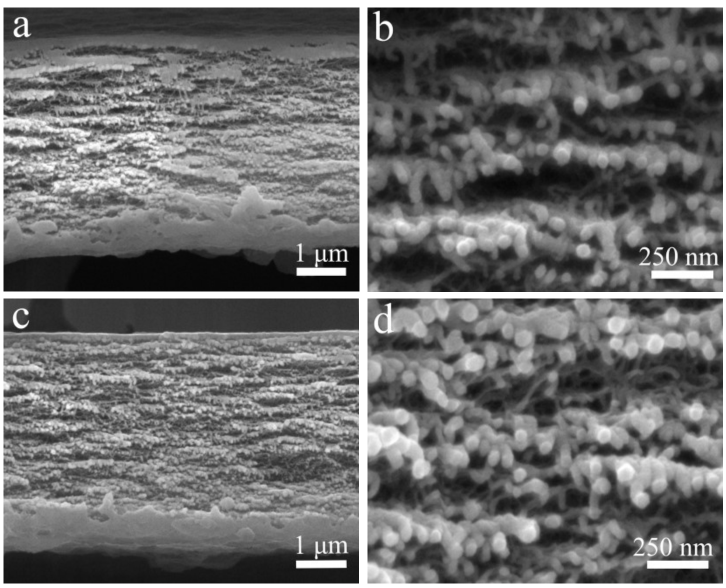

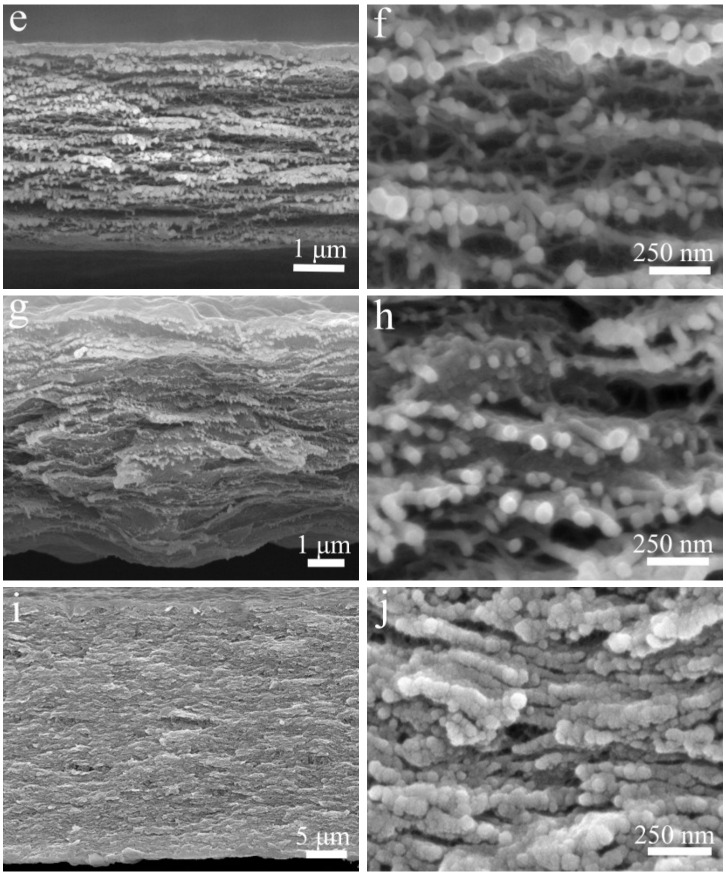

Figure S15. The SEM images of the fracture cross-section of a-b) ANF, c-d) ANF/PANI, e-f) ANF/rHGO, g-h) ANF/rHGO/PANI, i-j) rHGO/PANI films after tensile test.

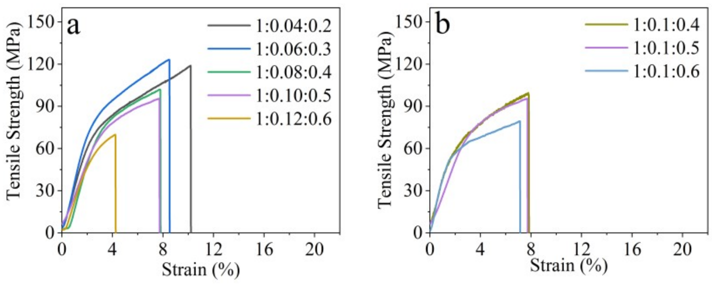

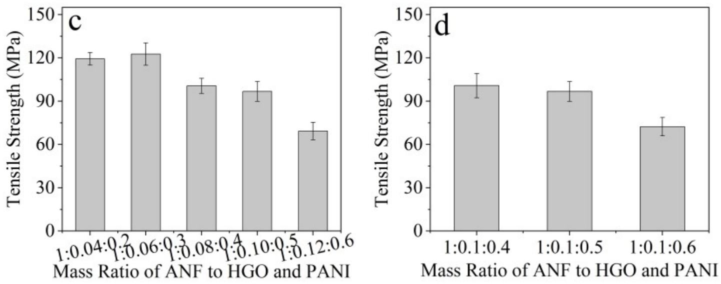

Figure S16. (a-b) Tensile strength test results and (c-d) averaged breaking tensile strength of ANF/rHGO/PANI composite samples with (a, c) different mass ratios (1:0.04:0.2, 1:0.06:0.3, 1:0.08:0.4, 1:0.10:0.5 and 1:0.12:0.6) of ANF, HGO and PANI and (b, d) different PANI contents (1:0.1:0.4, 1:0.1:0.5 and 1:0.1:0.6).

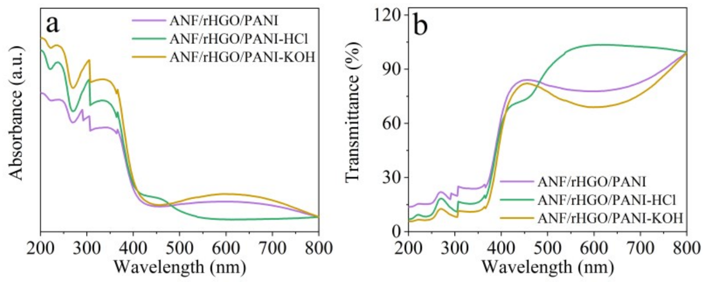

Figure S17. The UV-vis spectra of ANF/rHGO/PANI film post-treated by acidic or alkaline solution.

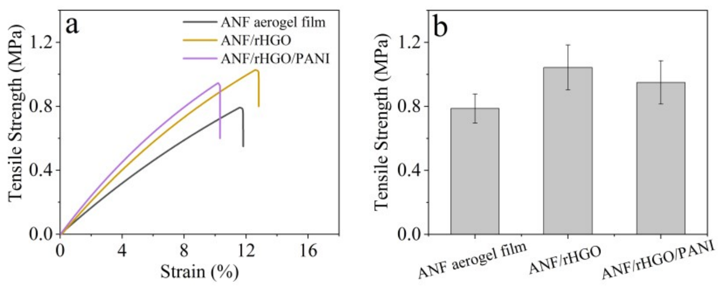

Figure S18. (a) The stress-strain curve and (b) averaged breaking tensile strength of

ANF, ANF/rHGO and ANF/rHGO/PANI aerogel film.

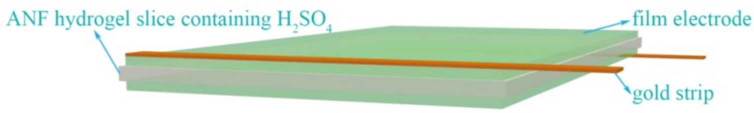

Figure S19. Schematic illustration for solid-state supercapacitor assembled using ANF/H_2SO_4 hydrogel slice separating as-prepared film electrodes.

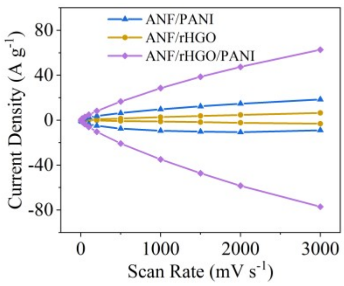

Figure S20. The plots of current density versus scan rate from CV curves.

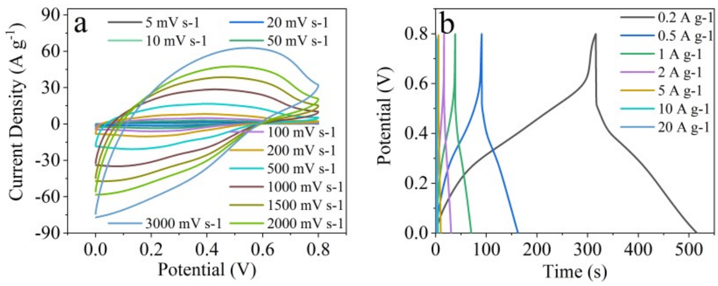

Figure S21. a) CV curves at various scan rates and b) GCD curves at various current densities for ANF/rHGO/PANI supercapacitor.

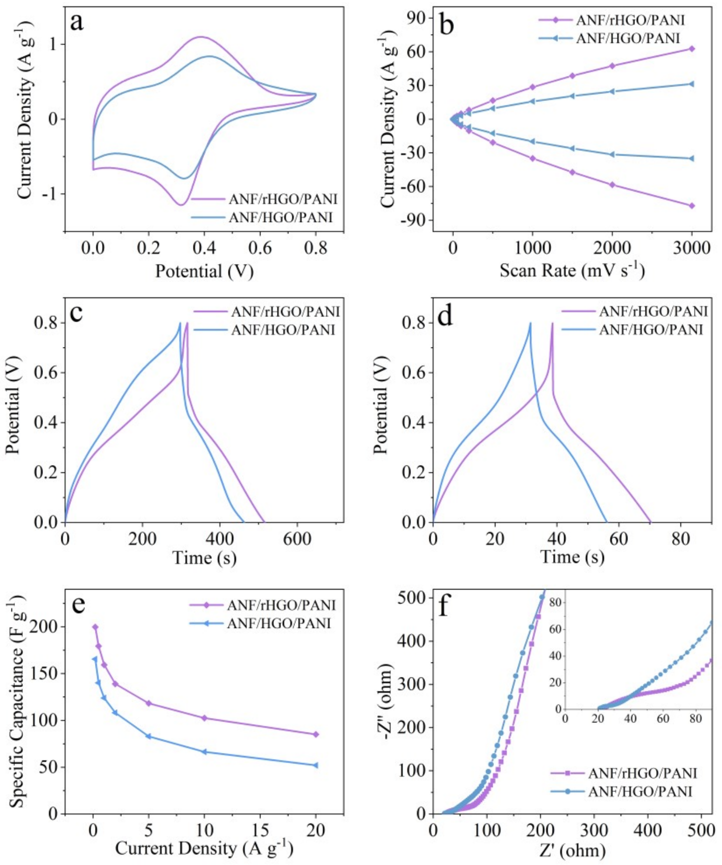

Figure S22. Electrochemical performance of ANF/rHGO/PANI and ANF/HGO/PANI supercapacitors: a) CV curves at 10 mV s^{-1}, b) The plot of current density versus scan rate from CV curves, c) GCD curves at 0.2 A g^{-1}, d) GCD curves at 1 A g^{-1}, e) Specific capacitance against current density, and f) EIS plot.

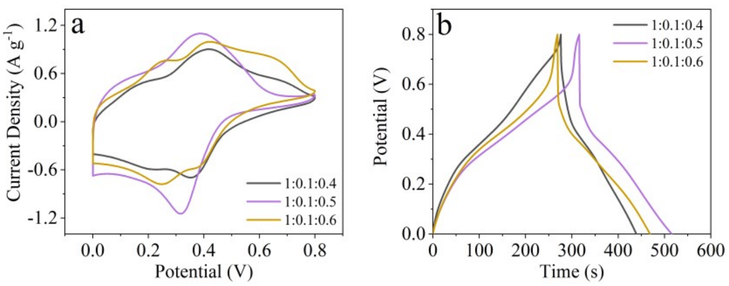

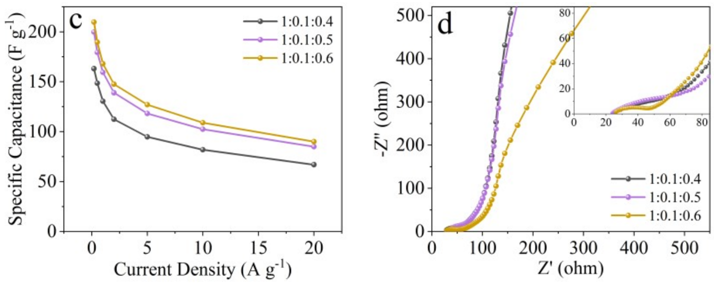

Figure S23. Electrochemical performance of ANF/rHGO/PANI composite supercapacitors with different PANI contents in composites: a) CV curves at 10 mV s^{-1}, b) GCD curves at 0.2 A g^{-1}, c) Specific capacitance against various current densities, and d) EIS plots.

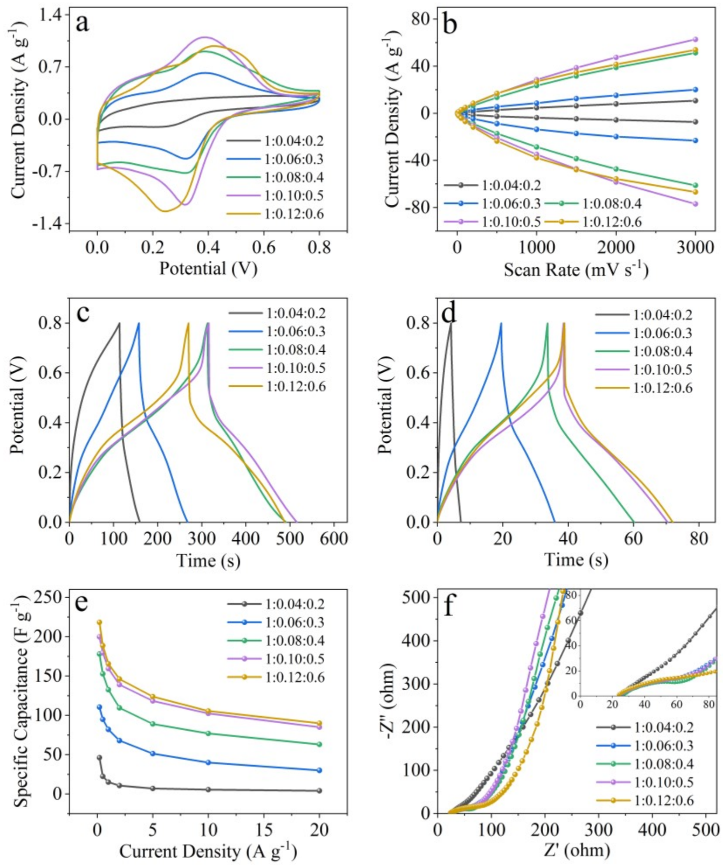

Figure S24. Electrochemical performance of ANF/rHGO/PANI composite supercapacitors with different mass ratios of ANF, HGO and PANI: a) CV curves at 10 mV s^{-1}, b) The plots of current density versus scan rate from CV curves, c) GCD curves at 0.2 A g^{-1}, d) GCD curves at 1 A g^{-1}, e) Specific capacitance against various current densities, and f) EIS plots.

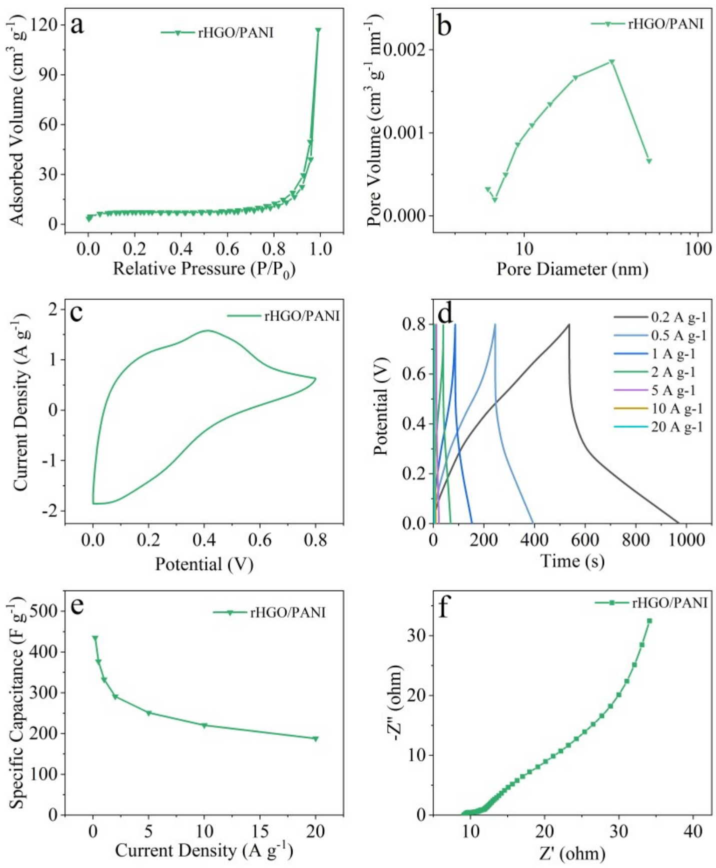

Figure S25. a) Adsorption-desorption isotherm curves, and b) the pore size distribution by the BJH method. c-f) The electrochemical performance of rHGO/PANI supercapacitor: c) CV curve at 10 mV s^{-1}, d) GCD curves at different current densities, e) Specific capacitance against current density, and f) EIS plot.

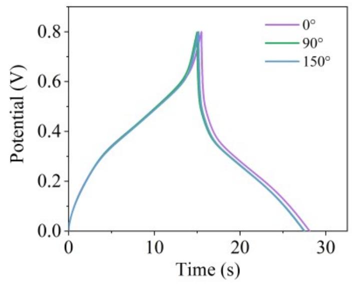

Figure S26. GCD curves at 2 A g^{-1} under different bending angles (0, 90 and 150 °) for ANF/rHGO/PANI supercapacitors.

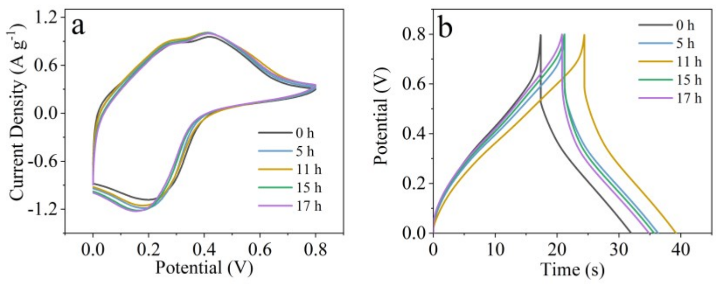

Figure S27. a) CV curves at 10 mV s^{-1} and b) GCD curves at 2 A g^{-1} for different times under keeping tensile force of 25 g for ANF/rHGO/PANI supercapacitors.

Table S1. The data of FT-IR spectra for the functional groups of as-prepared samples.

Assignment	**Wavenumbers (cm^{-1})**		
	ANF	**ANF/rHGO**	**ANF/rHGO/PANI**
C=O stretching vibrations	1655.6	1653.7	1652.3
C=C stretching vibrations of quinoid and benzenoid rings in PANI	--	--	1594.4, 1514.9
N-H deformation vibrations	1556.3	1542.8	1543.3
C-N stretching of aromatic amine	1316.7	1317.2	1315.8
C-C ring stretching vibrations	1268.9	1265.1	1268.9
C-O-C stretching vibrations	--	1108.9	1109.4
C-O stretching vibrations	1017.8	1017.3	1017.3
In-plane and out-of-plane bending vibrations of C-H	825.4	823.0	824.9

Table S2 Elemental Composition of XPS analysis for as-prepared samples.

Samples	C (at.%)	N (at.%)	O (at.%)
ANF	79.7	9.3	11.0
ANF/PANI	80.7	10.0	9.3
ANF/HGO	79.6	6.6	13.8
ANF/rHGO	80.0	8.5	11.5
ANF/HGO/PANI	80.5	9.5	10.0
ANF/rHGO/PANI	81.0	9.6	9.4

Table S3 C 1s spectra of C species in as-prepared samples, relative ratio (at.%)

Samples	C 1s					
	C-C/C=C	C-N	C-O	C=N	C=O	π-π*
ANF	39.4	31.3	--	--	22.9	6.4
ANF/PANI	41.9	24.1	--	13.9	9.7	10.4
ANF/HGO	43.1	20.5	18.6	--	11.5	6.3
ANF/rHGO	44.2	21.5	11.8	--	12.6	9.9
ANF/HGO/PANI	46.9	19.9	7.7	8.2	8.1	9.2
ANF/rHGO/PANI	47.8	20.7	5.8	6.9	8.9	9.9

Table S4 The tensile strength results of ANF based materials in literatures.

Sample	**Tensile strength (MPa)**	**Methods**	**Ref.**
ANF, 22% PPy/ANFs film	125±8 at 10.2±1.6% 80±5 at 13.6±1.9%	Py in-situ polymerization in ANF and filtration	S1
ANF, 20% BNNS@PDA/ANF film	93.5 at 21.3% 48 at 15%	BNNS@PDA into ANF with a homogenizer and filtration	S2
1% ANF, 20wt%-CNT FC-ANF/CNT aerogel films	1.8 at 10% 3.4 at 8%	ANF/CNT dispersion coated on Al foil to form hydrogel	S3
ANF, RGO/1wt%ANF films	~95 at 2%, 41.7±2.0 at 1.2%	GO/DMSO, ANF/DMSO mixed and filtration; 40 mg, 10-20 μm	S4
0.4 wt% ANF aerogel fiber	0.55 at 22%	~300 μm	S5
0.7 wt% ANFGS/PMMA film (ANFGS:ANFS/GO=2:1)	63.2 at 4.1%	ANFGS:GO/DMSO, ANF/DMSO mixed and centrifugation ANFGS/PMMA: solution casting method	S6
8 wt% ANF ANF/CNT (1:20)	855.7 ± 18.9 818.4 ± 16.2 at 2%	Wet Spinning: 8 wt% ANF dispersion and 0.6 wt% CNT aqueous solutions	S7
0.1 wt% BANF	138 ± 5.3 at 9%	aniline was polymerized in the	S8

73 wt% BANF/SWCNTs/15 wt% PANI film	40 ± 4 at 1.8%	presence of BANFs and single-walled carbon nanotubes	
KNFs ~6.60 wt% PDMS/PVDF@KNFs membrane	72 at 19% 90 at 20%	KNFS hydrothermal treatment, evenly dispersed by stirring and mixed with PVDF and PDMS	S9
SEBS/Kevlar/Ag/PVA fiber	35 at 220%	repeating adsorption and in situ reduction steps	S10
0.015% ANF 20%ANFs/80%PEDOT:PSS film	147.3 ± 7.1 at 3.8% 76.4 ± 2.5 at 2.2%	PEDOT:PSS into ANF/DMSO with a homogenizer and filtration	S11
1% ANF/EP plastic	83.3 ± 2.4 at 4%	ANF into EP with a homogenizer, adding curing agent for molding	S12
2% KNA KNA/PEG aerogel film	1.27 at 12.9% 2.1 at 20%	KNA aerogel films: freeze-drying KNA/PEG: KNA films were immersed in melting PCM and cooled to room temperature	S13
2 wt% ANF 34.7 vol% Au-ANF film	196 at 16.1% 96 at 9.1%	Spin coating to deposit ANF film, vacuum filtration to add Au NPs	S14
1.5 wt% ANF 40.9 wt% PANI/ANF film	185 at 11% 179 at 17.5%	Spin coating to deposit ANF film, and vacuum filtration to add PANI	S15
0.5 mg/mL ANF papers ANF-MXene/AgNW papers (20 wt% MXene/AgNW)	235.9 at 24.8% 155 at 13%	ANF hydrogel: vacuum filtrate ANF (DMSO) ANF-MXene/AgNW: vacuum filtrate to deposite MXene/AgNW	S16
Kevlar fibers 38.1% rGO hydrogel-Kevlar fibers	2.0 MPa m^3 kg^{-1} at 2.7% 1.6 MPa m^3 kg^{-1} at 2.7%	Kevlar fibers were aligned inside the tube and mixed with GO dispersion to hydrothermal react	S17
ANFW (water) Membranes ANFE (ethanol) Membranes	203.92 at 1.96% 141.34 at 3.28%	ANFs-DMSO dispersion was blended with a given ration followed by a desired amount of DI water or ethanol to substitute DMSO and precipitate the ANFs	S18
0.1% ANF aerogel (axial direction) ANF aerogel (radial direction)	0.095 ± 0.003 at 70% 0.165 ± 0.005 at 70% (compression)	ANF dispersion: $CaCl_2$, DME, PPD and TPC were added in NMP in turn, and diluted by NMP ANF aerogel: filtration and filtration	S19

0.2% ANF film 4.6 wt% PANI@ANF film	255.1 ± 7.1 at 18% 233.3 ± 6.1 at 17.5%	ANF dispersion vacuum filtrate and dry, and ANF film immerse in the PANI dispersion	S20
PMF film (5.7 wt% Au/ANF)	14.42 at 5.25%	PA was added into the ANF solution, and Au NP solution was added, then filtration	S21
MXene/11% ANF membrane (ANF 1%)	101 at 4.6%	MXene (DMSO), ANF (DMSO) with a homogenizer and filtration	S22
PPH	5.3 MPa at 250%	Polymerization of Ani in PVA and ABA	S23
1.0% ANF **ANF/rHGO** **ANF/rHGO/PANI film**	**105.4 at 8.72%** **121.4 at 9.0%** **95.5 at 7.7%**	**ANF, HGO and PANI mixed and adding water, hydrothermal**	**This work**

Table S5 The comparison of electrochemical performance of ANF/rHGO/PANI supercapacitor with reported results in literature.

Samples	**C_s**	**Test system**	**Ref.**
RGO/1wt% ANF	171 F g^{-1}, 0.5 A g^{-1} 155 F g^{-1}, 10 mV s^{-1}	Two-electrode	S4
25wt%TRGO/ANF	116 μF cm^{-2}, 10 mV s^{-1}	Three-electrode	S24
rGO($ANF_{2wt\%}$) hydrogel	~158 F g^{-1}, 5 mV s^{-1}	Two-electrode	S25
ANF Sheath on Dry-Spun CNT Wires	0.75 mF cm^{-1}, 3.25 μA cm^{-1}	Solid state supercapacitor	S7
38.1% rGO hydrogel-Kevlar cloth	~50 F g^{-1}, 1 A g^{-1}	Solid state supercapacitor	S17
20 wt%ANFs/PEDOT:PSS	111.5 F g^{-1}, 0.5 mA cm^{-3} 12.8 F g^{-1}, 0.1 A cm^{-3}	Three-electrode Solid state supercapacitor	S11
PANI/BANF/12wt% CNT	~210 F g^{-1}, 0.5 A g^{-1} ~180 F g^{-1}, 10 mV s^{-1}	Two-electrode	S8

4.6wt% PANI@ANF film	441.0 F g^{-1}, 1 A g^{-1}	Three-electrode	S20
	138 F g^{-1}, 0.5 A g^{-1}	Solid state supercapacitor	
62.5wt%ANF/rHGO/PANI	**200 F g^{-1}, 0.2 A g^{-1}**	**Solid state supercapacitor**	**This work**
	193 F g^{-1}, 10 mV s^{-1}		

References

[S1] X. Han, L. Lv, D. Yu, X. Wu and C. Li. *ACS Appl. Mater. Interfaces*, **2019**, *11*, 3466-3473.

[S2] T. Ma, Y. Zhao, K. Ruan, X. Liu, J. Zhang, Y. Guo, X. Yang, J. Kong and J. Gu. *ACS Appl. Mater. Interfaces*, **2020**, *12*, 1677-1686.

[S3] P. Hu, J. Lyu, C. Fu, W. B. Gong, J. Liao, W. Lu, Y. Chen and X. Zhang. *ACS Nano*, **2020**, *14*, 688-697.

[S4] S. R. Kwon, J. Harris, T. Zhou, D. Loufakis, J. G. Boyd and J. L. Lutkenhaus. *ACS Nano*, **2017**, *11*, 6682-6690.

[S5] Z. Liu, J. Lyu, D. Fang and X. Zhang. *ACS Nano*, **2019**, *13*, 5703-5711.

[S6] J. Fan, Z. Shi, L. Zhang, J. Wang and J. Yin. *Nanoscale*, **2012**, *4*, 7046-7055.

[S7] W. Cao, L. Yang, X. Qi, Y. Hou, J. Zhu and M. Yang. *Adv Funct Mater*, **2017**, *27*, 1701061.

[S8] P. Flouda, A. H. Quinn, A. G. Patel, D. Loufakis, D. C. Lagoudas and J. L. Lutkenhaus. *Nanoscale*, **2020**, *12*, 16840-16850.

[S9] D. Li, X. Gou, D. Wu and Z. Guo. *Nanoscale*, **2018**, *10*, 6695-6703.

[S10] J. Li, L. Wang, X. Wang, Y. Yang, Z. Hu, L. Liu and Y. Huang. *ACS Appl.*

Mater. Interfaces, **2020**, *12*, 1427-1435.

[S11] Y. Li, G. Ren, Z. Zhang, C. Teng, Y. Wu, X. Lu, Y. Zhu and L. Jiang. *J. Mater. Chem. A*, **2016**, *4*, 17324-17332.

[S12] J. Lin, S. H. Bang, M. H. Malakooti and H. A. Sodano. *ACS Appl. Mater. Interfaces*, **2017**, *9*, 11167-11175.

[S13] J. Lyu, Z. Liu, X. Wu, G. Li, D. Fang and X. Zhang. *ACS Nano*, **2019**, *13*, 2236-2245.

[S14] J. Lyu, X. Wang, L. Liu, Y. Kim, E. K. Tanyi, H. Chi, W. Feng, L. Xu, T. Li, M. A. Noginov, C. Uher, M. D. Hammig and N. A. Kotov. *Adv Funct Mater*, **2016**, *26*, 8435-8445.

[S15] J. Lyu, X. Zhao, X. Hou, Y. Zhang, T. Li and Y. Yan. *Compos Sci Technol*, **2017**, *149*, 159-165.

[S16] Z. Ma, S. Kang, J. Ma, L. Shao, Y. Zhang, C. Liu, A. Wei, X. Xiang, L. Wei and J. Gu. *ACS Nano*, **2020**, *14*, 8368-8382.

[S17] W. Sun, S. A. Shah, J. L. Lowery, J. H. Oh, J. L. Lutkenhaus and M. J. Green. *Adv. Mater. Interfaces*, **2019**, *6*, 1900786.

[S18] Y. Wu, F. Wang and Y. Huang. *Polym. Composite*, **2019**, *40*, 2534-2538.

[S19] C. Xie, L. He, Y. Shi, Z. X. Guo, T. Qiu and X. Tuo. *ACS Nano*, **2019**, *13*, 7811-7824.

[S20] Q. Yin, H. Jia, A. Mohamed, Q. Ji and L. Hong. *Nanoscale*, **2020**, *12*, 5507-5520.

[S21] H. Zhang, L. Feng, Y. Liang and T. Xu. *Nanoscale*, **2019**, *11*, 437-443.

[S22] Z. Zhang, S. Yang, P. Zhang, J. Zhang, G. Chen and X. Feng. *Nat. Commun.*, **2019**, *10*, 2920.

[S23] W. Li, F. Gao, X. Wang, N. Zhang and M. Ma. *Angew Chem Int Ed*, **2016**, *55*, 9196-9201.

[S24] S. R. Kwon, M. B. Elinski, J. D. Batteas and J. L. Lutkenhaus. *ACS Appl. Mater. Interfaces*, **2017**, *9*, 17125-17135.

[S25] S. A. Shah, D. Kulhanek, W. Sun, X. Zhao, S. Yu, D. Parviz, J. L. Lutkenhaus and M. J. Green. *J Colloid Interface Sci*, **2020**, *560*, 581-588.